Translational Oncology
www.transonc.com

Volume 13 Number 1 January 2020 pp. 11–16 11

Cell Population Data–Driven Acute Promyelocytic Leukemia Flagging Through Artificial Neural Network Predictive Modeling

Rana Zeeshan Haider[*,‡], **Ikram Uddin Ujjan**[†] **and Tahir S. Shamsi**[*]

[*]Post-graduate Institute of Life Sciences, National Institute of Blood Disease (NIBD), Karachi, Pakistan; [†]Department of Basic Medical Sciences, Liaqat University of Health and Medical Sciences (LUMHS), Jamshoro, Pakistan; [‡]International Center for Chemical and Biological Sciences (ICCBS), University of Karachi, Karachi, Pakistan

Abstract

A targeted and timely offered treatment can be a benefitting tool for patients with acute promyelocytic leukemia (APML). Current round of study made use of potential morphological and immature fraction–related parameters (cell population data) generated during complete blood cell count (CBC), through artificial neural network (ANN) predictive modeling for early flagging of APML cases. We collected classical CBC items along with cell population data (CPD) from hematology analyzer at diagnosis of 1067 study subjects with hematological neoplasms. For morphological assessment, peripheral blood films were examined. Statistical and machine learning tools including principal component analysis (PCA) helped in the evaluation of predictive capacity of routine and CPD items. Then selected CBC item–driven ANN predictive modeling was developed to smartly use the hidden trend by increasing the auguring accuracy of these parameters in differentiation of APML cases. We found a characteristic triad based on lower (53.73) platelet count (PLT) with decreased/normal (4.72) immature fraction of platelet (IPF) with addition of significantly higher value (65.5) of DNA/RNA content–related neutrophil (NE-SFL) parameter in patients with APML against other hematological neoplasm's groups. On PCA, APML showed exceptionally significant variance for PLT, IPF, and NE-SFL. Through training of ANN predictive modeling, our selected CBC items successfully classify the APML group from non-APML groups at highly significant (0.894) AUC value with lower (2.3 percent) false prediction rate. Practical results of using our ANN model were found acceptable with value of 95.7% and 97.7% for training and testing data sets, respectively. We proposed that PLT, IPF, and NE-SFL could potentially be used for early flagging of APML cases in the hematology-oncology unit. CBC item–driven ANN modeling is a novel approach that substantially strengthen the predictive potential of CBC items, allowing the clinicians to be confident by the typical trend raised by these studied parameters.

Translational Oncology (2020) 13, 11–16

Introduction

Acute promyelocytic leukemia (APML) in comparison with other types of hematological neoplasms, particularly acute myeloid leukemia (AMLs) has highly bizarre clinical, morphological, and biological characteristics and requires a targeted therapy [1]. Start of the treatment without any delay for definitive diagnosis or other concerns is an effective approach in APML [2]. This is particularly because of life-threatening coagulopathy initiated by the abnormal promyelocytes (AP) [3]. The development of innovative technologies and analytical principles in flow cytometry has allowed the

Address all correspondence to: Rana Zeeshan Haider, Post-graduate Institute of Life Sciences, National Institute of Blood Disease (NIBD), ST 2/A, Block 17, Gulshan-e-Iqbal, KDA Scheme 24, Karachi, Pakistan. E-mail: zeeshan3335@yahoo.com
Received 29 July 2019; Accepted 24 September 2019

1936-5233/19
https://doi.org/10.1016/j.tranon.2019.09.009

Table 1. Mean (Along Standard Deviation) Values for Classical and Extended CBC Items Generated by Modern (Sysmex XN-1000) Hematology Analyzer Are Presented for Our Study Groups

CBC Parameters	APML (n=44) Mean±SD	AML (n=181) Mean±SD	CML (n=89) Mean±SD	MDS (n=51) Mean±SD	MDS/MPN (n=10) Mean±SD	MPN (n=71) Mean±SD	ALL (n=136) Mean±SD	HL (n=9) Mean±SD	NHL (n=91) Mean±SD	MM (n=32) Mean±SD	NC (n=349) Mean±SD
Hb	8.11±1.97	7.45±2.73	9.38±1.87	7.86±2.38	9.49±2.75	11.88±3.63	5.85±3.46	9.51±2.59	5.85±2.83	8.61±1.76	13.79±1.40
RBC(10^12/L)	3.38±1.96	3.57±2.44	3.49±0.80	2.63±0.90	3.48±0.75	4.79±1.81	5.29±3.01	3.87±1.06	7.98±4.16	3.20±0.87	4.79±0.49
PCV	25.60±5.29	25.09±8.09	28.86±6.24	23.91±7.20	29.5±7.14	37.70±11.91	24.73±7.63	29.55±8.26	32.28±7.95	26.62±5.40	41.72±4.04
MCV	88.18±8.06	90.34±10.47	83.45±10.14	92.63±9.23	85.2±9.37	81.28±11.02	83.94±9.12	76.67±8.50	87.33±9.27	87.28±9.76	87.22±3.66
MCH	29.01±3.05	29.39±3.53	27.09±3.90	30.15±3.64	26.9±3.93	25.37±4.16	27.36±2.91	24.22±2.54	27.17±3.34	27.64±3.42	28.82±1.22
MCHC	32.95±2.33	32.35±1.93	32.15±2.25	32.36±1.83	31.3±2.41	31.18±1.89	32.64±1.93	31.55±1.88	31.11±2.32	31.59±1.74	33.07±1.23
WBC(10^9/L)	26.80±47.65	39.66±66.75	192.39±142.46	6.54±9.86	40.20±19.32	18.09±22.44	70.91±107.47	7.75±4.92	76.63±114.68	7.11±3.50	7.53±1.40
PLT(10^3/uL)	**53.73±85.94**	**60.88±83.18**	438.42±292.94	115.98±149.65	240.9±622.72	**590.37±518.88**	**53.74±62.92**	145.44±143.31	163.78±114.13	217.19±89.35	268.42±57.10
Reticcount	1.15±1.51	1.93±11.84	3.13±2.21	1.82±1.73	2.79±2.38	2.31±1.7	0.55±1.07	1.79±1.57	0.48±0.85	1.53±0.99	0.44±0.67
NEUT#(10^3/uL)	10.35±18.81	9.59±29.59	161.65±125.42	3.40±5.33	23.59±15.33	13.79±19.42	3.25±4.22	5.37±3.62	5.30±4.60	4.53±3.32	4.32±1.05
LYMPH#(10^3/uL)	4.77±11.01	9.07±12.92	9.62±5.23	1.76±1.04	7.38±5.70	2.20±1.45	47.76±77.40	1.38±1.93	64.94±107.52	1.80±0.89	2.38±0.59
MONO#(10^3/uL)	12.05±25.11	21.29±42.93	8.25±8.81	1.25±4.58	8.80±9.28	1.03±1.51	20.09±42.26	0.96±0.78	6.03±14.99	0.57±0.28	0.54±0.12
EO#(10^3/uL)	0.07±0.15	0.18±0.99	5.10±5.24	0.11±0.32	0.57±1.24	0.73±2.18	0.13±0.29	0.03±0.06	0.26±0.37	0.14±0.14	0.24±0.149
BASO#(10^3/uL)	0.06±0.13	0.07±0.21	5.32±5.22	0.04±0.142	0.19±0.18	0.14±0.20	0.15±0.39	0.02±0.01	0.12±0.20	0.02±0.02	0.03±0.01
NEUT%(%)	35.91±19.93	22.16±19.90	81.92±11.61	42.32±20.22	57.41±19.29	67.44±18.15	13.11±17.24	70.82±11.86	18.61±20.30	59.44±17.32	57.06±6.82
LYMPH%(%)	37.91±26.65	37.90±22.28	7.19±5.86	44.36±22.17	17.77±7.87	21.87±17.46	64.36±22.07	15.65±15.31	69.50±25.55	29.44±15.18	31.87±6.45
MONO%(%)	25.37±21.72	39.09±23.60	4.88±4.61	11.49±9.29	21.99±19.06	6.90±4.20	21.07±18.04	12.85±5.29	10.92±16.12	8.79±4.13	7.36±1.50
EO%(%)	0.71±1.50	0.67±2.07	3.16±5.51	1.37±1.62	2.2±5.70	3.03±2.61	0.49±0.95	0.5±0.78	0.74±1.35	2.04±1.99	3.20±1.89
BASO%(%)	0.10±0.16	0.18±0.36	2.85±2.04	0.45±1.04	0.63±0.87	0.76±0.75	0.22±0.30	0.17±0.16	0.22±0.31	0.28±0.23	0.49±0.25
IG#(10^3/uL)	1.53±3.76	1.86±4.83	65.04±57.26	0.49±1.65	7.51±6.22	1.71±4.82	0.73±1.51	0.19±0.29	0.44±1.42	0.13±0.24	0.02±0.01
IG%(%)	5.08±7.77	4.38±6.33	30.31±9.61	3.23±5.21	17.75±10.53	5.00±7.23	1.76±2.93	2.07±1.74	1.03±2.47	1.56±2.19	0.37±0.25
RDW-SD(fL)	53.09±11.30	57.63±13.88	58.2±10.32	59.49±19.31	58.58±10.95	54.59±15.22	53.92±13.24	43.67±17.42	51.41±12.56	53.70±14.71	42.98±3.72
RDW-CV(%)	17.02±3.44	18.08±4.16	20.12±2.84	18.62±5.96	19.66±4.32	20.17±5.21	18.66±3.99	18.94±3.66	16.70±3.75	18.45±4.18	13.56±0.98
NRBC#(10^3/uL)	0.11±0.22	0.35±1.06	2.16±3.42	1.38±8.87	0.97±1.6	0.13±0.29	0.51±1.56	0.02±0.05	0.10±0.39	0.01±0.02	0.01±0.01
NRBC%(%)	0.91±1.35	1.61±3.55	1.15±1.38	3.63±16.20	3.39±7.62	1.02±2.29	1.40±3.87	0.21±0.34	0.38±1.41	0.18±0.43	0.01±0.02
IPF(%)	4.72±1.57	**8.35±5.59**	5.55±2.83	**15.61±7.73**	4.30±1.36	4.41±2.02	6.53±3.15	**0.90±0.3**	4.52±2.38	3.34±1.52	3.70±2.28
		Low		Very Low		High		Very High			

For quick visual identification of "hot" and "cold" spots in reference to normal control color-shading (blue for low and red for high count) approach is used.Hb, hemoglobin; RBC, red blood cell; PCV, pack cell volume; MCV, mean cell volume; MCH, mean cell hemoglobin; MCHC, mean cell hemoglobin concentration; WBC, white blood cell; PLT, platelet; NEUT#, absolute neutrophil count; LYMPH#, absolute lymphocyte count; MONO, absolute monocyte count; EO#, absolute eosinophil count; BASO#, absolute basophil count; NEUT%, neutrophil percent; LYMPH%, lymphocyte percent; MONO%, monocyte percent; EO%, eosinophil percent; BASO%, basophil percent; IG#, absolute immature granulocyte count; IG%, immature granulocyte percent; RDW, red cell distribution width; NRBC#, absolute nucleated red blood cell count; NRBC%, nucleated red blood cell percent; IPF, immature platelet fraction; MM, multiple myeloma.

Table 2. Values of CBC-Based White Cell Scattering (Morphological) Items Among Study Groups

CBC Parameters	APML (n=44) Mean±SD	AML (n=181) Mean±SD	CML (n=89) Mean±SD	MDS (n=51) Mean±SD	MDS/MPN (n=10) Mean±SD	MPN (n=71) Mean±SD	ALL (n=136) Mean±SD	HL (n=9) Mean±SD	NHL (n=91) Mean±SD	MM (n=32) Mean±SD	NC (n=349) Mean±SD
[NE-SSC(ch)]	143.08±10.87	140.81±14.05	149.05±6.53	141.28±13.12	139.8±12.90	149.21±6.87	149.64±9.26	148.97±2.78	149.76±8.52	152.03±4.50	149.62±4.92
[NE-SFL(ch)]	65.5±22.55	51.66±17.53	45.86±5.12	45.29±7.41	47.9±14.02	43.30±5.20	50.71±8.30	48.41±4.19	46.84±8.36	46.80±6.94	45.25±3.28
[NE-FSC(ch)]	72.59±11.81	72.29±11.15	84.04±5.57	75.37±8.32	74.06±10.44	80.22±6.15	80.89±7.03	81.82±5.54	80.94±7.13	83.04±4.53	85.37±4.25
[LY-X(ch)]	84.50±10.35	87.33±10.38	81.63±8.89	81.63±2.05	82.1±6.26	80.49±4.43	84.75±7.25	83.77±3.37	80.67±5.86	81.02±1.97	81.46±2.83
[LY-Y(ch)]	65.54±9.37	68.65±12.29	42.89±19.68	67.60±4.72	59.21±7.51	63.89±4.79	68.91±16.15	71.27±7.47	60.96±8.99	64.14±4.92	65.30±4.32
[LY-Z(ch)]	57.32±3.018	56.67±3.74	52.44±3.49	56.53±2.53	56.26±2.31	55.97±1.81	58.20±3.79	60.54±2.52	57.70±2.83	56.61±1.88	58.41±2.85
[MO-X(ch)]	120.75±9.83	118.05±8.27	126.30±6.91	119.12±5.82	121.83±7.93	119.75±4.90	110.20±7.39	124.52±4.04	111.81±6.79	118.88±4.32	119.27±2.68
[MO-Y(ch)]	115.35±25.35	114.64±23.51	112.09±24.26	109.12±22.12	109.62±21.11	103.04±14.44	108.43±23.79	121.84±11.52	102.51±12.06	100.23±13.07	104.10±7.74
[MO-Z(ch)]	65.49±7.91	62.66±4.97	60.28±2.89	63.45±4.98	62.15±2.71	61.16±3.76	65.29±6.54	64.57±3.50	64.61±5.07	64.04±2.79	65.431±2.94
[NE-WX]	419.16±119.61	435.71±127.01	501.29±76.69	410.86±105.92	466.8±56.02	362.56±83.42	386.72±108.57	328.44±37.05	330.6±66.40	317.41±22.01	305.28±16.27
[NE-WY]	1262.53±829.70	1388.88±755.01	2467.68±693.20	919.65±463.28	1890.6±558.12	882.45±453.96	1226.47±616.40	670.11±50.98	781.88±325.88	675.75±121.78	608.44±27.69
[NE-WZ]	801.79±213.15	825.50±257.67	847.02±109.49	731.74±160.64	870.9±135.64	675.18±105.61	721.081±203.64	638.78±36.45	663.47±195.27	619.78±36.64	612.41±39.70
[LY-WX]	550.86±136.81	533.66±118.75	695.52±168.56	527.08±100.73	631.9±166.034	533.37±90.25	535.53±119.28	532.67±114.59	541.02±127.24	505.75±79.93	492.23±45.96
[LY-WY]	994.91±184.93	1069.66±267.75	1929.71±1070.73	982.76±200.60	1232.1±290.37	1020.48±214.96	1060.03±231.82	949.89±185.18	987.39±207.88	931.34±144.41	921.46±81.60
[LY-WZ]	586.67±142.48	568.05±115.83	801.74±165.36	510.35±120.03	633.8±116.38	543.24±135.97	578.50±138.35	541.55±134.57	489.85±115.09	460.28±42.82	454.51±31.87
[MO-WX]	301.81±104.41	340.51±75.02	357.22±65.23	294.57±84.68	310.9±95.68	300.15±71.56	319.04±90.03	269.89±40.01	288.59±66.54	263.62±58.25	250.18±27.93
[MO-WY]	701.67±446.57	873.84±282.05	1146.87±346.87	696.59±316.55	881.7±219.30	779.08±252.55	878.07±317.66	714.89±108.46	801.84±235.03	665.56±181.16	682.73±83.91
[MO-WZ]	601.16±204.80	616.05±112.94	767.94±100.79	564.41±161.06	655.8±112.47	629.94±130.85	681.88±226.76	581.44±61.21	629.46±253.11	545.06±78.11	532.88±61.29
		Low		Very Low		High		Very High			

NE-SSC, neutrophils cell complexity; NE-SFL, neutrophils fluorescence intensity; NE-FSC, neutrophils cell size; LY-X, lymphocytes cell complexity; LY-Y, lymphocytes fluorescence intensity; LY-Z, lymphocytes cell size; MO-X, monocytes cells complexity; MO-Y, monocytes fluorescence intensity; MO-Z, monocytes cell size; NE-WX, neutrophils complexity and the width of dispersion; NE-WY, neutrophils fluorescence intensity and the width of dispersion; NE-WZ, neutrophils cell size and the width of dispersion; LY-WX, lymphocytes complexity and width of dispersion; LY-WY, lymphocytes fluorescence intensity and the width of dispersion; LY-WZ, lymphocytes cell size and the width of dispersion; MO-WX, monocytes complexity and the width of dispersion; MO-WY, monocytes fluorescence intensity and the width of dispersion; MO-WZ, monocytes cell size and the width of dispersion; MM, multiple myeloma.

commercialization of new-generation hematological analyzers. These are capable to generate data about the morphological characteristics and immature fractions of blood cells termed as "cell population data" (CPD) along with classical complete blood cells (CBC) count parameters. CPD items have a high degree of analytical efficiency for identifying many cellular abnormalities and can be used for the screening of several hematological and nonhematological disorders [4–8].

The aim of this study was to evaluate the clinical utility of WBC morphology (CPD) parameters in early premicroscopic differentiation of APML. Apart from the microscopic classification systems and its limitations, we worked to propose a novel prediction model based on artificial neural network (ANN); multilayer perceptron (MLP) that would utilize routinely generated scattering items along with CBC testing. We hypothesized that an ANN-based model built on CPD items would enhance predictive ability of these morphological parameters and this kind of modeling can be incorporated in real-time clinical practice.

Materials and Methods

We clinically evaluated CPD items generated by one of flow cytometry–based hematology analyzer (Sysmex XN-1000, Kobe, Japan) in peripheral blood for early premicroscopic exclusion of APML from other common hematological neoplasms. From January 2014 to July 2017, a total of 1067 patients with 44 APML (PML-RARA), 181 AML (excluded APML), 89 chronic myeloid leukemia (CML), 51 myelodysplastic syndrome (MDS), 71 myeloproliferative disorders (MPN) except CML, 10 MDS/MPN, 136 acute lymphocytic leukemia (ALL), 9 Hodgkin's lymphoma (HL), 95 non-Hodgkin's lymphoma (NHL), 32 multiple myeloma, and 349 normal control were prospectively enrolled at the National Institute of Blood Disease and Bone Marrow Transplantation (NIBD & BMT) Karachi, Pakistan. Flow cytometry–based modern hematology analyzer (Sysmex XN-1000) was used for CBC testing of 1067 blood samples. Demographic features, classical CBC items, and CPD parameters were compared between the study groups. To explore the subtle pattern and to generate better predictive model on

significantly deviated CBC items (PLT, immature platelet fraction (IPF), and NE-SFL), we used unsupervised machine learning tool (principal component analysis [PCA]) and MLP analysis, one of the common types of ANN. It performed prediction and classification along with generation of predicted-by-observed chart, ROC curve, cumulative gains, and lift charts for MLP. The Institutional Review Board of NIBD and BMT approved this study (permit number: NIBD/RD-167/14-2014).

Results

From routine and extended CBC parameters (Table 1), values of platelet count and IPF showed characteristic trend for APML group against other study groups. Although individually lower values for platelet count or IPF is noted in various study groups as in APML but none of these group showed decrease/near normal value of IPF in demand of such degree of thrombocytopenia. While among white cell morphological items, patients with APML showed significantly higher value for NE-SFL (side fluorescent light intensity) compared with its corresponding hematological neoplasms (Table 2).

We conducted PCA to visualize a typical trend of IPF in lower platelet count along with higher values of NE-SFL for APML against its peer study groups. As shown in Figure 1, APML showed significant variance in comparison with other hematological neoplasms and found on upper extreme left end of PCA pilot. Triad of IPF, plate count, and NE-SFL successfully differentiate APML from other study groups (Figure 1).

The summary of MLP model (Figure 2) to challenge the typical trend of NE-SFL, platelet count, and IPF for prediction of patients with APML showed various positive signs as "cross entropy error" with smallest error (20.73) for testing data set. In addition to that, it

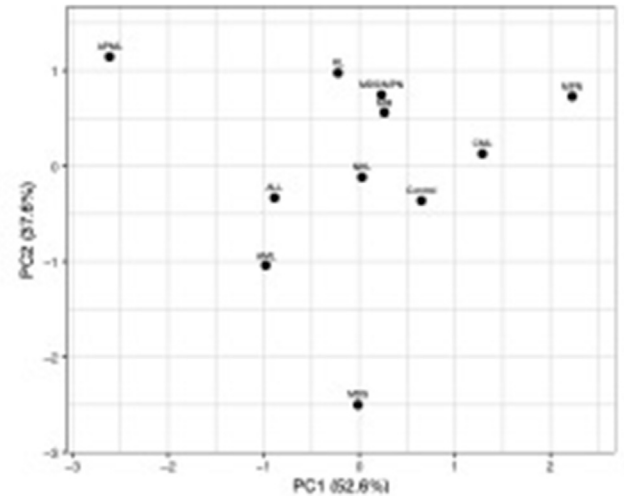

Figure 1. Visualization of latent pattern of selected (PLT, IPF, and NE-SFL) CBC parameters for study groups through principal component analysis (PCA). By unsupervised machine learning tools (PCA) three-dimensional data reduced into two dimensions so that we can plot and understand our data in a better way. Together, both components (PC1 and PC2) covered 90.2% of the information (variance). In plot, groups are labeled with their names.

Model Summary

Training	Cross Entropy Error	92.715
	Percent Incorrect Predictions	4.3%
Testing	Cross Entropy Error	20.734
	Percent Incorrect Predictions	2.3%

Case Processing Summary

		N	Percent
Sample	Training	729	73.3%
	Testing	266	26.7%
Valid		995	100.0%
Excluded		72	
Total		1067	

Classification

Sample	Observed	Predicted		
		Non-APML	APML	% Correct
Training	Non-APML	698	0	100.0%
	APML	31	0	0.0%
	Overall %	100.0%	0.0%	95.7%
Testing	Non-APML	260	0	100.0%
	APML	6	0	0.0%
	Overall %	100.0%	0.0%	97.7%

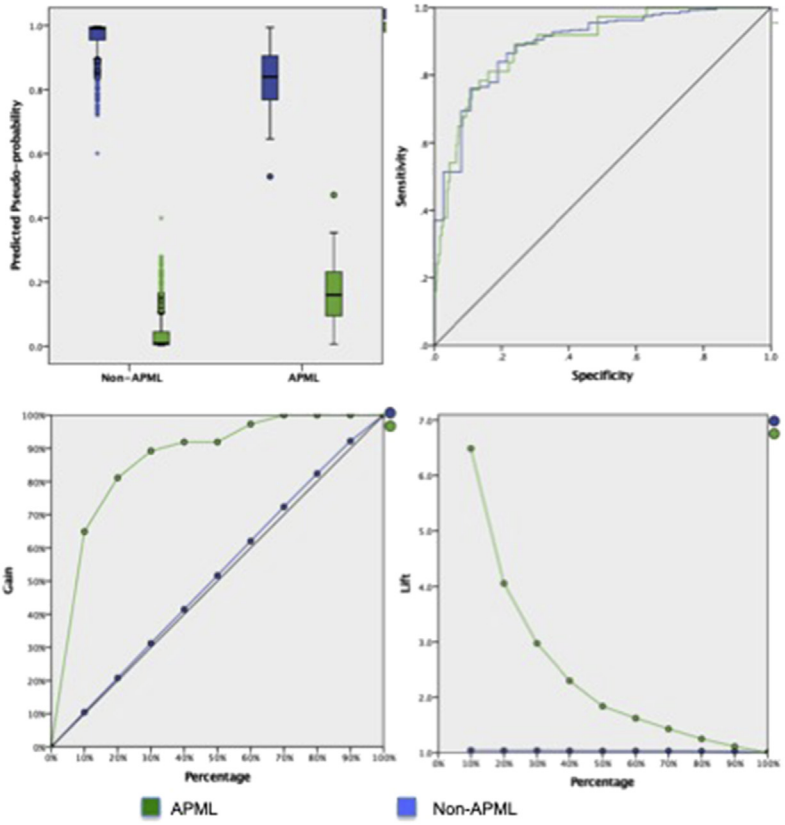

Figure 2. The model summary, classification table, predicted-by-observed chart, ROC curve, cumulative gains and lift chart for multilayer perceptron for APML *vs.* non-APML.

also showed notably lower percentage of incorrect predictions as a whole and particularly for testing (2.3%) as compared with training data set (4.3%). Practical results of using the MLP network were acceptable with 95.7% and 97.7% for training and testing data sets, respectively, as shown in classification table (Figure 2). A visual look of ROC curve and 0.894 AUC value further endorsed the predictive ability of the network.

The predicted-by-observed chart (Figure 2) for the combined training and testing samples displayed predicted pseudoprobabilities as clustered boxplots. All boxplots were found symmetrical about the horizontal line at 0.5 mark. The cumulative gains chart showed notable trend that if we score a data set with the network and sort all the cases by predicted pseudoprobability of APML, we can expect top 10% to contain approximately 65% of all the cases considering the APML category (Figure 2). The lift chart provides (Figure 2) us a different look on cumulative gains chart; the lift at 10% for the category APML is 65%/10% = 6.5. We must know that both cumulative and lift charts are based on combined testing and training samples.

Discussion

Clinically, APML represents a hematologic emergency that enforces a rapid exclusion for a quick start of its treatment, even before molecular and cytogenetic diagnosis (PML-RARA rearrangement). CPD items generated by hematology analyzers have a strong potential for being introduced as automated morphological items for detection of changes in WBC white cell's morphology. Various studies were conducted to evaluate clinical utility of CPD items for early exclusion of hematological disorders. A study by Yang et al. evaluated white cell scattering items for differentiation of acute leukemia lineage by using Coulter DxH800 analyzer. In this study, the authors derive 21-item−based model and reported very high (100%) specificity and sensitivity for differentiation of APML cases, whereas for ALL, comparatively less-significant specificity and sensitivity was achieved [4]. In another study by Virk et al., the clinical utility of the white cell scattering items, scattergrams, and flags for screening of AML cases with significant specificity was published [9].

In this study, we found an interesting "triad", that is a fraction of immature platelets (IPF) remained decreased or normal in response to thrombocytopenia (lower platelet count) and NE-SFL came with significantly higher values in patients with APML. Higher values of NE-SFL may be justified by an increased infiltration of immature hyperactive (AP) having higher RNA/DNA content than other immature and mature cells that falsely counted in neutrophil area. Increased destruction along with suppression of platelet production may partly explain the low platelet count and decreased IPF value (near normal) in regard to severity of thrombocytopenia. Hence, we propose the use of platelet count, NE-SFL, and IPF as criteria for early flagging of APML, which will enforce the rapid and targeted peripheral film examination for APs and subsequent diagnostic workup. Here, it is also clear that this criterion cannot be used as diagnostic parameters because it is confirmed by PML-RARA.

Through this study, we have also demonstrated the clinical utility of applying machine learning tools in predictive modeling on data generated with CBC test, which in our hands could be used as morphological parameters for premicroscopic exclusion and guide the further diagnostic workup of APML. On peripheral blood film's microscopic images, by using image processing tools (image segmentation, feature extraction, cell identification, and other) and ANN-based modeling, various studies were conducted. These studies include the classification of acute lymphocytic leukemic (ALL) cells from healthy cells [10−15], acute myeloid leukemic (AML) cells from healthy cells [16,17], and WBCs grouping into various classes of AML, ALL, and their French-American-British (FAB) subtypes [18−26]. To our knowledge, this is the first study for CPD-driven flagging of APML through an ANN predictive modeling. We suggest that an ANN-based modeling would be able to smartly recognize the typical patterns in selected CBC items for differentiation of APML cases more accurately. Eventually, if successful, CBC (routine, extended, and CPD) items through ANNs could be incorporated into hematology laboratory decision support/information system for flagging of APML. As a future work, this approach could be studied in an extended way by using WBC, red blood cell (RBC), and platelet morphological and immature fraction parameters for short and targeted diagnostic workups especially in common (regional) blood disorders.

Conclusion

A characteristic triad of lower platelet counts with decreased fraction of immature platelet (IPF) along higher value for DNA/RNA content−related neutrophil (NE-SFL) parameter is illustrated for flagging of APML. −driven-driven−The platelet, IPF, and NE-SFL values driven ANN modeling is a novel approach that substantially strengthen the flagging potential of these parameters in augur of APML cases. This approach could potentially reduce the frequency of extra and irrational diagnostic tests, which is time-consuming and extra burden on patients. Hence, the proposed selected CBC item−driven predictive modeling can be used as an assistant diagnostic tool in decision support system of hematology laboratory and clinic for screening of APML.

Author contribution

R.Z.H. conducted the experiments, collected and analyzed the data under supervision of I.U. and T.S.S.; I.U., T.S.S., and R.Z.H. wrote the paper. All authors read and approved the final manuscript.

Conflicts of interest

Authors have no conflict of interest.

Ethics approval

The Institutional Review Board of NIBD, Karachi, Pakistan (Permit number: NIBD/RD-167/14-2014).

Acknowledgements

The authors are grateful to laboratory members of clinical hematology laboratory, NIBD for assistance in patient's diagnosis.

References

[1] Lee H-J, Park H-J, Kim H-W and Park S-G (2013). Comparison of laboratory characteristics between acute promyelocytic leukemia and other subtypes of acute myeloid leukemia with disseminated intravascular coagulation. *Blood Res* **48**(4), 250−253.

[2] Sanz MA, Grimwade D, Tallman MS, Lowenberg B, Fenaux P and Estey EH, et al (2008). Guidelines on the management of acute promyelocytic leukemia: recommendations from an expert panel on behalf of the European LeukemiaNet. *Blood 2008.*

[3] Abedin S and Altman JK (2016). Acute promyelocytic leukemia: preventing early complications and late toxicities. *ASH Educ Program B* **2016**(1), 10−15.

[4] Yang JH, Kim Y, Lim J, Kim M, Oh E-J and Lee H-K, et al (2014). Determination of acute leukemia lineage with new morphologic parameters available in the complete blood cell count. *Ann Clin Lab Sci* **44**(1), 19−26.

[5] Haschke-Becher E, Vockenhuber M, Niedetzky P, Totzke U and Gabriel C (2008). A new high-throughput screening method for the detection of chronic lymphatic leukemia and myelodysplastic syndrome. *Clin Chem Lab Med* **46**(1), 85−88.

[6] Silva M, Fourcade C, Fartoukh C, Lenormand B, Buchonnet G and Callat M, et al (2006). Lymphocyte volume and conductivity indices of the haematology analyser Coulter® GEN. STM in lymphoproliferative disorders and viral diseases. *Int J Lit Humanit* **28**(1), 1−8.

[7] Miguel A, Orero M, Simon R, Collado R, Perez PL and Pacios A, et al (2007). Automated neutrophil morphology and its utility in the assessment of neutrophil dysplasia. *Lab Hematol: Off Publ Int Soc Lab Hematol* **13**(3), 98−102.

[8] Park SH, Kim H-H, Kim I-S, Yi J, Chang CL and Lee EY (2016). Cell population data NE-SFL and MO-WX from sysmex XN-3000 can provide additional information for exclusion of acute promyelocytic leukemia from other acute myeloid leukemias: a preliminary study. *Annal Lab Med* **36**(6), 607−610.

[9] Virk H, Varma N, Naseem S, Bihana I and Sukhachev D (2019). Utility of cell population data (VCS parameters) as a rapid screening tool for Acute Myeloid Leukemia (AML) in resource-constrained laboratories. *J Clin Lab Anal* **33**(2):e22679.

[10] Mohapatra S, Patra D and Satpathy S (2014). An ensemble classifier system for early diagnosis of acute lymphoblastic leukemia in blood microscopic images. *Neural Comput Appl* **24**(7−8), 1887−1904.

[11] Amin MM, Kermani S, Talebi A and Oghli MG (2015). Recognition of acute lymphoblastic leukemia cells in microscopic images using k-means clustering and support vector machine classifier. *J Med Signals Sensors* **5**(1), 49.

[12] Li Y, Zhu R, Mi L, Cao Y and Yao D (2016). Segmentation of white blood cell from acute lymphoblastic leukemia images using dual-threshold method. *Comput Math Meth Med* **2016**.

[13] Rawat J, Singh A, Bhadauria H, Virmani J and Devgun JS (2017). Computer assisted classification framework for prediction of acute lymphoblastic and acute myeloblastic leukemia. *Biocybernetics Biomed Eng* **37**(4), 637−654.

[14] Bigorra L, Merino A, Alférez S and Rodellar J (2017). Feature analysis and Automatic identification of leukemic lineage blast cells and reactive lymphoid cells from peripheral blood cell images. *J Clin Lab Anal* **31**(2): e22024.

[15] Rehman A, Abbas N, Saba T, SIu Rahman, Mehmood Z and Kolivand H (2018). Classification of acute lymphoblastic leukemia using deep learning. *Microsc Res Tech* **81**(11), 1310−1317.

[16] Agaian S, Madhukar M and Chronopoulos AT (2014). Automated screening system for acute myelogenous leukemia detection in blood microscopic images. *IEEE Syst J* **8**(3), 995−1004.

[17] Kazemi F, Najafabadi TA and Araabi BN (2016). Automatic recognition of acute myelogenous leukemia in blood microscopic images using k-means clustering and support vector machine. *J Med Signals Sensors* **6**(3), 183.

[18] Gonzalez JA, Olmos I, Altamirano L, Morales BA, Reta C and Galindo MC, et al (2011). Leukemia identification from bone marrow cells images using a machine vision and data mining strategy. *Intell Data Anal* **15**(3), 443−462.

[19] Putzu L, Caocci G and Di Ruberto C (2014). Leucocyte classification for leukaemia detection using image processing techniques. *Artif Intell Med* **62**(3), 179−191.

[20] Madhloom HT, Kareem SA and Ariffin H (2015). Computer-aided acute leukemia blast cells segmentation in peripheral blood images. *J Vibroeng* **17**(8), 4517−4532.

[21] Neoh SC, Srisukkham W, Zhang L, Todryk S, Greystoke B and Lim CP, et al (2015). An intelligent decision support system for leukaemia diagnosis using microscopic blood images. *Sci Rep* **5**, 14938.

[22] Priya DK, Krithiga S, Pavithra P and Kumar JR (2015). Detection of leukemia in blood microscopic images using fuzzy logic. *Int J Eng Res Sci Technol* **240**, 197−205.

[23] Rawat J, Singh A, Bhadauria H and Virmani J (2015). Computer aided diagnostic system for detection of leukemia using microscopic images. *Procedia Comp Sci* **70**, 748−756.

[24] Reta C, Altamirano L, Gonzalez JA, Diaz-Hernandez R, Peregrina H and Olmos I, et al (2015). Correction: segmentation and classification of bone marrow cells images using contextual information for medical diagnosis of acute leukemias. *PLoS One* **10**(7):e0134066.

[25] Hu SB, Wong DJ, Correa A, Li N and Deng JC (2016). Prediction of clinical deterioration in hospitalized adult patients with hematologic malignancies using a neural network model. *PLoS One* **11**(8):e0161401.

[26] Singh G, Bathla G and Kaur S (2016). Design of new architecture to detect leukemia cancer from medical images. *Int J Appl Eng Res* **11**(10), 7087−7094.